Modeling and Simulation of Microstructure Formation for Porosity Prediction in Thermal Barrier Coatings Under Air Plasma Spraying Condition

K. Bobzin, N. Bagcivan, D. Parkot, M. Schäfer, and I. Petković

Effective physical and mechanical properties of thermal barrier coatings are strongly dependent on the coating microstructure. The main objective of this study is the coating porosity prediction during the coating formation by simulation. For this purpose, two simulation approaches are presented. The first model takes into account physical impact, deformation, and overlying of powder particles on the solid substrate. Therefore, computational fluid dynamics and the volume of fluid method for this model were used. In the second approach, a faster and therefore more efficient model was developed, hence it was strongly simplified to simulate the formation of coatings and their microstructure. The splat formation was handled by calculating the flattening degree as a function of the Reynolds number. The disc-shaped particles were discretized by cuboids. The neighboring cuboids are moveable against each other at their contact areas. The displacement of those depends on material properties and the Reynolds number as well. Both approaches for predicting the microstructure were mutually compared.

Keywords	air plasma spraying, coating properties, numerical simulation, particle impact

1. Introduction

Plasma spraying is a complex process with many parameters influencing the coating properties. The influencing parameters can be assigned to three characteristic process parts, where they can be controlled. The first process part is the generation of the plasma in the torch, where plasma enthalpy can be controlled varying gas mixture and electric power. The second part considers powder particle in plasma, where they are injected, heated, melted, and accelerated to the substrate. Third part includes coating formation on the substrate by impact, spreading, and solidification of the particles (Ref 1). Solidified particles, in literature known as splats or lamellas, build a coating layer including pores or voids, which can be found mostly at the edges of the splats. Therefore, the final microstructure of the plasma sprayed coating is inhomogeneous and exhibits porosity. Sometimes it includes even unmolten particles. Such coating inhomogeneities influence various physical and mechanical coating

K. Bobzin, N. Bagcivan, D. Parkot, M. Schäfer, and **I. Petković**, Surface Engineering Institute, RWTH Aachen University, Aachen, Germany. Contact e-mail: schaefer@iot.rwth-aachen.de.

properties which are strongly linked to the final morphology of the individual splats (Ref 2-4).

In this work, thermal barrier coatings (TBCs) were considered. TBCs deposited by plasma spraying are widely used in many industrial applications such as thermal protection of gas turbine blades as well as cylinders and valves of diesel engines (Ref 5). In most cases, partially yttria stabilized zirconia (PYSZ, $ZrO_2 + 7$-8% Y_2O_3) is used as material for TBCs, because of its high temperature phase stability and low thermal conductivity. Typical TBC coatings have thicknesses of about 300 μm. The splats morphology, responsible for the final coating properties, depends on many parameters such as substrate surface properties, particle velocity, temperature, and melting state prior to impact on the substrate surface. In industrial applications, substrate temperatures are adjusted to obtain appropriate coating porosity. In order to reduce the coating porosity, substrate is being preheated. On the other hand, it can be cooled with the opposite aim—to achieve a higher coating porosity, which increases its thermal protection capability (Ref 6).

In recent years, splat morphologies of diverse powder materials were investigated experimentally and numerically by many scientists. An excellent overview to splat formation under thermal spray conditions has been given in Ref 4. Salimijazi et al. (Ref 7) showed the effect of the surface temperature and roughness on a single PYSZ splat morphology by experiments. Parizi et al. (Ref 8) used numerical simulations with volume of fluid method for predictions of splats on patterned substrate surfaces. The numerical results were correlated with experiments and showed a good matching. Most of the numerical models

are based on classical computational fluid dynamics (CFD). This method calculates accurate results, but at high computational effort. Therefore, there is still a lack of proper models for the simulation of a realistic coating microstructure. One interesting example of alternatives to the CFD method was presented in Ref 9. The splat morphologies were investigated with CFD and used as a basis for a Monte Carlo model for microstructure prediction of the complete coating in 2D.

The goal of this work is to compare the predictions of the splat morphologies and the porosities obtained by CFD model and newly developed, so called simplified microstructure prediction (SMP) model. The SMP-Model should be prework for the simulation of the complete coating microstructure in 3D considering air plasma spraying (APS) process conditions.

2. CFD Model

2.1 Theoretical Background

The model of PYSZ particle impact is based on the numerical solution of the time dependent conservation equations discretized using finite difference method on a three-dimensional Cartesian grid. The grid represents a small part of space before the substrate including substrate surface, which was assumed as flat. The fluid was assumed as Newtonian, incompressible with laminar flow. The influence of the surrounding gas was not taken into account. Tracing of the transient free surfaces of molten particle was modeled by the volume of fluid (VoF) method. The VoF method is based on the solution of transport equation for the volume fraction, formulated as:

$$\frac{\partial F}{\partial t} + \nabla \cdot (Fu) = 0 \tag{Eq 1}$$

where u is fluid velocity and F is the fluid volume fraction in the cells in the computational grid. Values of F are one for a cell full of fluid and zero for empty cells. For cells containing the free surfaces, F has values between zero and one. The mass and momentum conservation equations can be expressed as:

$$\nabla \cdot u = 0 \tag{Eq 2}$$

$$\rho \left(\frac{\partial u}{\partial t} + u \cdot \nabla u \right) = -\nabla p + \mu \nabla^2 u + Fvol + S \tag{Eq 3}$$

where ρ is fluid density and p is pressure. For this model, the temperature dependent dynamic viscosity according to

$$\mu = 0.1 \cdot \exp(-2.95 + 5993/T_p) \tag{Eq 4}$$

as presented in Ref 10 was used. Here and further, T_p is particle temperature. The force $Fvol$ in Eq 3 is amount of body force acting on the fluid. In this case as body force only the influence of the surface tension σ was considered. The term S on the right hand side of Eq 3 is the drag force, which increases with the solidified fraction f_s in the mushy zone, up to large values. When the particle material is fully

solidified, S tents to infinity and therefore the material flow will "freeze." This term is formulated as:

$$S = \frac{f_s^2}{(1 - f_s)^3} u \tag{Eq 5}$$

The energy conservation equation

$$\rho \left(\frac{\partial H}{\partial t} + u \nabla H \right) = \nabla \cdot (\lambda \nabla T_p), \tag{Eq 6}$$

where λ is thermal conductivity, was used to model the heat transfer inside of particle material. The enthalpy

$$H = CpT_p + (1 - f_s)L \tag{Eq 7}$$

depends on the solidification ratio and is assumed to be a linear function of the temperature T_p. Here C_p is specific thermal capacity. The latent heat L in this model is released between liquids temperature T_{liq} and solidus temperature T_{sol} controlled with solid fraction of fluid f_s (Ref 11).

Convective heat transfer on the interface between particle material and substrate surface is:

$$q = \frac{T_P - T_S}{R_C} \tag{Eq 8}$$

where T_S is substrate temperature and R_C is thermal contact resistance per unit area between particle and substrate. The R_C is dependant on time, interface position between particle material and substrate but also on substrate roughness (Ref 12). According to Ref 2 and 10, the values of R_C vary between 10^{-6} for poor contact and 10^{-8} for good contact. However, in this model, a constant value of R_C corresponding to perfect wetting was used (see Table 1). The above presented equations were solved with the commercial CFD Software Flow-3D version 9.3.

2.2 Boundary and Initial Conditions

The dimensions of the cuboid-shaped calculation domain for the particle impact were set to $146 \times 146 \times 160 \ \mu m^3$. Initial position, velocities, diameters, and temperatures of the particles are presented in Table 1. In this model, relative low values of initial particle velocities (Table 1) were taken to avoid particle material splashing

Table 1 Simulation setup of the three particles

	Particle 1	Particle 2	Particle 3
v_p, m/s	29	24	21
T_p, K	3000		
D_0, μm	30	40	50
Re	128.5	141.8	155.1
x-Position, μm	15	15	-15
y-Position, μm	15	-15	-15
z-Position, μm	125		
ξ_m	1.85	1.88	1.90
ρ, kg/m^3	5700		
σ, J/m^2	0.5		
μ, kg/m s	$0.1 \cdot \exp(-2.95 + 5993/T_p)$		
R_C, W/m^2	10^{-8}		

during the spreading and provide an appropriate splat form for a comparison with the results of the SMP-Model. The initial particle velocity vectors were set perpendicular to the substrate surface. The generation of the three particles in the calculation domain was carried out by user-defined subroutine, allowing generation of large number of varying fluid shapes in the calculation domain. All information, as position, size, temperature, velocity of fluids, and time of the fluid generation can be given in an external matrix. In this case, the matrix had following information. The diameters of spherical particles were taken as 30, 40, and 50 μm consequently, and the time period between the particles was 0.0001 s. The time period of 0.0001 s was assumed to be enough for the full solidification of a particle, before the next particle is generated.

All faces of the calculation domain were defined as outflow boundary condition, except the face on the bottom of the calculation domain (according to the z-direction, which is perpendicular to the bottom face). This face builds the substrate and was defined as immobile no-slip and no-penetration wall boundary. The value of R_C in (13) was provided as an input parameter in the model and was set to a constant value considering perfect wetting based on Ref 2. At the free surface of the droplet and on the remaining substrate area not covered by the droplet adiabatic boundary conditions were assumed. The effect of the surrounding gas was neglected in the whole calculation domain. The value of substrate temperature $T_S = 300$ K was assumed to be constant.

3. Simplified Microstructure Prediction-Model (SMP-Model)

The SMP-Model calculates the microstructure development during coating formation under plasma spraying condition. Splat formation is based on the model of Madejski (Ref 13) and the particles were discretized by cuboids, which are able to perform a movement relative to each other.

The position, temperature, velocity, and diameter have to be determined as input parameter for each particle, as in the CFD-Model. Additionally, essential material properties are needed.

3.1 Splat Formation

Powder particles or droplets are impacting perpendicularly on the surface, which is the first assumption. Impact behavior of droplets can be categorized into rebound, deposition and splashing addicted to the Sommerfeld parameter K as a function of the Weber and Reynolds number:

$$K = \sqrt{We} \cdot \sqrt[4]{Re}. \qquad (\text{Eq } 9)$$

This parameter was initially investigated by Mundo et al. (Ref 14, 15). Splashing occurs, at least for ethanol and water droplets, for a Sommerfeld parameter greater

than 57.7 (Ref 16). Fukumoto et al. (Ref 17) introduced a new criterion for calculating a critical value K_f when splashing occurs, taking the substrate temperature T_s into account. This critical value can be expressed as:

$$K_f = 0.5 \cdot m^{1.25} \cdot Re^{0.3} \cdot K \qquad (\text{Eq } 10)$$

where m is the ratio of maximum radial flattening velocity v_f to particle velocity v_p ($m = v_f/v_p$) (Ref 17). The maximum flattening velocity v_f changes with substrate temperature T_S. For values of $K_f > 7$ during the particle impact material splashing occurs.

3.2 Flattening Degree

The maximum flattening degree

$$\xi_m = \frac{D}{D_0} \qquad (\text{Eq } 11)$$

describes the ratio of D, the deformed disc-shaped particle after collision with the substrate, were D_0 is the initial particle diameter. Jones (Ref 18) developed the first analytical model which describes the flattening degree on a smooth surface as a function of surface tension and viscosity by neglecting solidification. Madejski (Ref 13) developed the model of Jones further by considering solidification. This model ends up with a relation were the flattening degree is a function of the Reynolds number only:

$$\xi_m = a \cdot Re^b. \qquad (\text{Eq } 12)$$

According to Madejski, this expression gives good results for $Re > 100$, $a = 1.2941$, and $b = 0.2$. Later other authors, summarized in Ref 2, developed similar models for predicting the flattening degree. All of them result in an expression like the one above, were $a = 0.8$ to 1.2941 and $b = 0.125$, 0.167, or 0.2.

3.3 Discretization of the Powder Particles

The deformed, disc-shaped, powder particles were discretized by cuboids. Every cuboid has the same size $\delta \cdot \delta \cdot h$ (see Fig. 1). The height h of a cuboid is equal to the resulting height of the deformed powder particle. The diameter of the particle was divided, along the particle's axis of symmetry into an even number n (Fig. 1).

Here, $\vec{v}_P$ is the velocity of the particle perpendicular to the substrate prior impact. The position of each particle is linked to the δ-stepped grid.
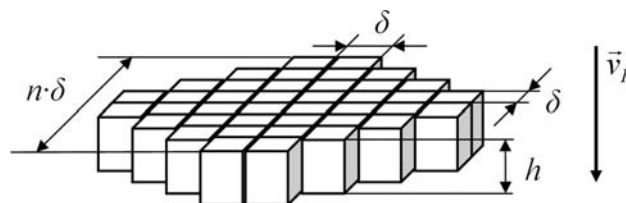

Fig. 1 Exemplarily discretized particle

3.4 Relative Displacement of the Cuboids at Their Contact Areas

The cuboids can be displaced relative to each other in normal direction to the substrate as presented in Fig. 2 (in direction of the surface normal vector $\vec{S}$). The maximum displacement was described by the value Ψ_i for each particle i.

The value of Ψ (Eq 13) was calculated before the particle impacting on the surface:

$$\Psi = C_M \frac{v_p \cdot \rho}{\mu}. \qquad \text{(Eq 13)}$$

The proportionality constant C_M depends on material properties and is given in units of area, hence, Ψ result in units of length.
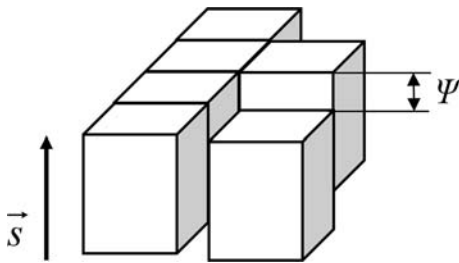
Fig. 2 Example for one movable cuboid

4. Comparison of the Simulation Results

The calculation setups for both simulations, the CFD and the SMP-Model, are equal and summarized in Table 1. As described above, three particles were simulated. The diameters of those three particles are taken from a standard powder grain fraction between 10 and 60 μm (Ref 19). The values for surface tension, density, and dynamic viscosity for both models are taken from Ref 10.

The velocities have been chosen to get a Sommerfeld K parameter below 57.7 and to get according to Fukumoto $K_f < 7$, to prevent splashing. The flattening degree was calculated with value of $a = 0.82$ and $b = 0.167$.

4.1 Simulation Results of the CFD-Model and the SMP-Model

The simulation results of the CFD-Model as well as of the SMP-Model are visually and analytically compared. At first isometric and top view are compared (Fig. 3).

The calculation time for the simulation of the CFD-Model was about 12 h. The simulated time was 0.0003 s. In Fig. 4, the time frames of the simulation of the three impacting particles are presented. The time period of 0.0001 s between the particle generation appears to be well estimated, which means that the particles are fully solidified before the following particle impact.

For the correlation with the results of the SMP-Model, the cross section parallel to the x-z-plane at $y = -2 \times 10^{-6}$ m of the overlaid splats, presented in Fig. 5(a),
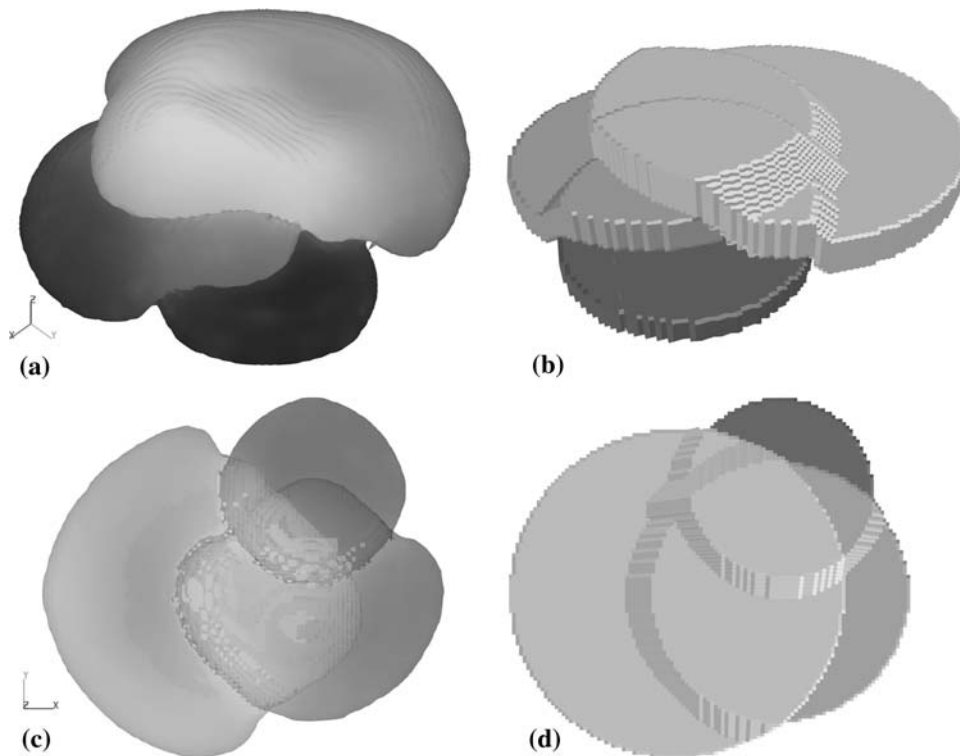

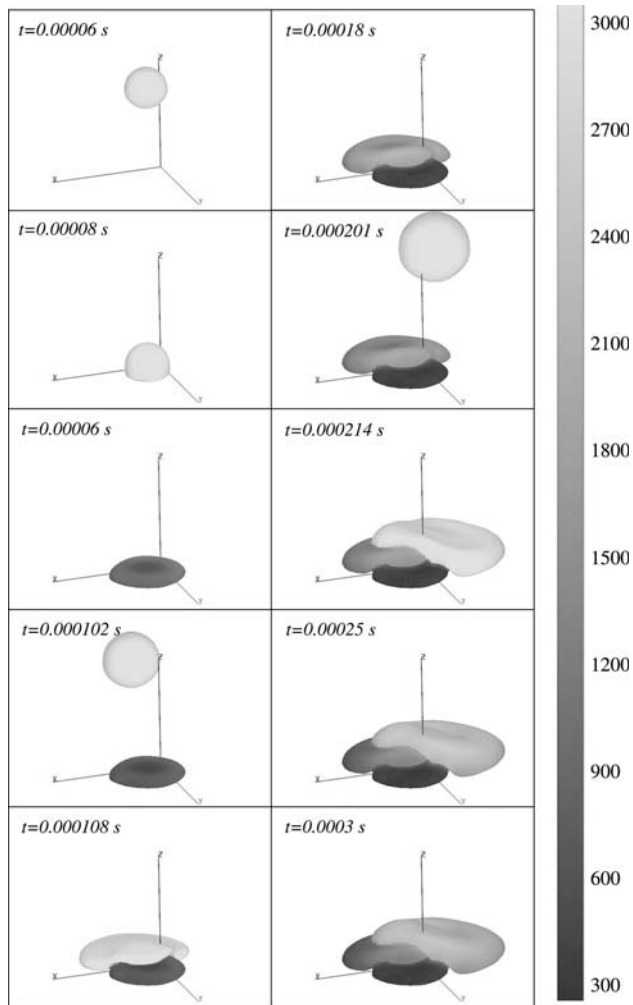**Fig. 3** Comparison of CFD- and SMP-Model, isometric and top view

Fig. 4 Time frames of the particles impact

Fig. 5 Cross section of the overlaid particles

was used. The low values of the initial velocities resulted in pores between the individual particles. In Fig. 5, three characteristic pores, marked as A_1, A_2, and A_3, can be seen. In order to correlate porosity of both simulation approaches, the values of the pore areas were determined as: $A_1 = 16.89$, $A_2 = 16.89$, and $A_3 = 32.56$ μm². The sum of the porosity in the above cross section (Fig. 5) is 4.8%.

The computation time of the SMP-model was about 1/4000 of the time taken by the CFD-Model. The domain was discretized in 2 μm sections tangential to the substrate and in 0.1 μm sections normal to the substrate. The maximum deviation of the flattening degree is 1.5%, compared to the CFD simulation. The height of each particle is smaller than in the CFD-Model, because of the difference between the particle's cross-sectional areas. In the CFD-Model, the edges at the free surface of the particles are rounded, but in SMP-Model those edges are sharp.

The porosity of the considered cross section in Fig. 6(a) is equal to 3.3%. The porosity, marked as A_1-A_3 in Fig. 6(a), have the absolute values of $A_1 = 15.9$ μm², $A_2 = 15.9$ μm², and $A_3 = 31.3$ μm². Because of the different
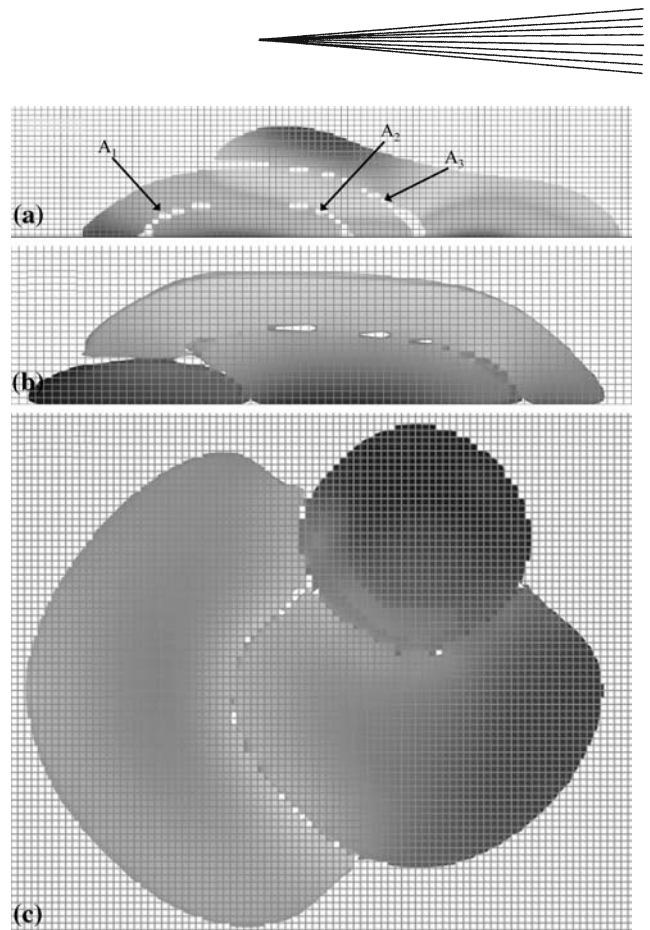
assumptions of the models, the pores result in different shapes. This can be explained with disc-shaped particle assumption in the SMP-Model. But the values of characteristic porosity areas for both models are similar.

The advantage of a three-dimensional model is the almost infinite amount of comparable cross sections. Two cross sections are presented in Fig. 5(b) and (c) as well as Fig. 6(b) and (c) to verify the optical identicalness. One can see the effect of the assumption in the SMP-Model that the spreading of the particle is calculated before impact.

The shape of the first particle impacting on the substrate result in a circular form. The following particles are impacting partially on solidified particles. This results in a non circular deformation in the CFD simulation, contrary to the basic assumption of a circular shape of the SMP-Model (Fig. 5 and 6).

5. Conclusion

Two different numerical approaches to calculate coating porosity are presented in this work. The first one, using the CFD method, is based on the numerical solution of the governing conservation equations of the particle impact on the solid substrate. With this model, an impact of three particles was calculated and analyzed. To avoid splashing of particle material, during the impact and allow the
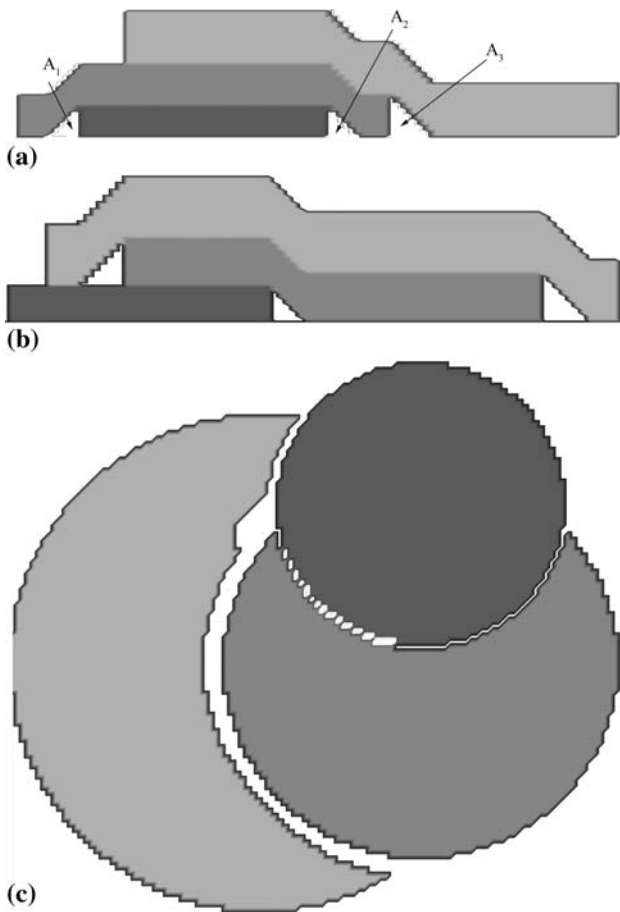
Fig. 6 Cross section of the domain, parallel to the *x-z* plane, 2 μm in *y* direction, parallel to the *y-z* plane, 2 μm in *x* direction and parallel to the *x-y* plane, 8 μm in *z* direction

correlation with the SMP-Model, low particle velocities were considered in the simulation. The low velocities have caused obvious characteristic pores on the particle interfaces. These three characteristic areas in the CFD results were determined for the comparison with results of the SMP-Model.

The second model, the SMP-Model calculates the impact and overlaying of discretized splat-discs on the substrate. The SMP-Model is a fast tool for predicting the distribution of pore accumulations and the resulting shape of the coating surface. By the factor Ψ the impact velocity, inertial and viscous forces are taken into account. For slow impact velocities, this model results in deviant cross sections of the particles compared to their real behavior, because the height reduces with growing radius of a particle. The three marked areas, which compose the porosity of 2.9%, is 1.9 percentage points less compared to the CFD-Model.

Acknowledgment

References

1. P. Fauchais, Understanding Plasma Spraying, *J. Phys. D: Appl. Phys.*, 2004, **37**, p R86-R108
2. P. Fauchais, M. Fukumoto, A. Vardelle, and M. Vardelle, Knowledge Concerning Splat Formation: An Invited Review, *J. Therm. Spray Technol.*, 2004, **13**(3), p 337-360
3. R. Nickel, "Die beschichtungsprozessabhängige Materialmodellierung von EB-PVD- und APS-Wärmedämmschichten," PhD Thesis, Surface Engineering Institute, RWTH Aachen, 2007, p 3-14
4. S. Chandra and P. Fauchais, Formation of Solid Splats During Thermal Spray Deposition, *J. Therm. Spray Technol.*, 2009
5. S. Ahmaniemi, J. Tuominen, M. Vippola, P. Vuoristo, T. Mäntylä, F. Cernuschi, C. Gualco, A. Bonadei, R. Di Maggio, and S. Ahmaniemi, Characterization of Modified Thick Thermal Barrier Coatings, *J. Therm. Spray Technol.*, 2004, **13**(3), p 361-369
6. A. Zagorski, F. Szuecs, V. Balaschenko, S. Siegmann, N. Margandant, and A. Ivanov, Experimental Study of substrate thermal conditions at APS and HVOF, *Proceeding of the 2003 International Thermal Spray Conference*, Orlando, Florida, USA, 2003, p 1255-1260
7. H.R. Salimijazi, L. Pershin, T.W. Coyle, J. Mostaghimi, S. Chandra, Y.C. Lau, L. Rosenzweig, and E. Moran, Effect of Droplet Characteristics and Substrate Surface Topography on the Final Morphology of Plasma-Sprayed Zirconia Single Splats, *J. Therm. Spray Technol.*, 2007, **16**(2), p 291-299
8. H.B. Parizi, L. Rosenzweig, J. Mostaghimi, S. Chandra, T. Coyle, L. Pershin, A. McDonald, and C. Moreau, Numerical Simulation of Droplet Impact on Patterned Surfaces, *J. Therm. Spray Technol.*, 2007, **16**(5), p 713-721
9. T. Steinke and M. Bäcker, Monte Carlo Simulation of Thermal Sprayed Coatings, *Proceeding of the 2006 International Thermal Spray Conference*, Seattle, Washington, USA, 2006
10. M. Vardelle, A. Vardelle, A.C. Leger, P. Fauchais, and D. Gobin, Influence of Particle Parameters at Impact on Splat Formation and Solidification in Plasma Spraying Processes, *J. Therm. Spray Technol.*, 1994, **4**, p 50-58
11. M.R. Barkhudarov and C.W. Hirt, Casting Simulation: Mold Filling and Solidification-Benchmark Calculations Using FLOW-3D, *Modeling of Casting, Welding, and Advanced Solidification Processes VII*, 1993, p 935-946
12. M. Pasandideh-Fard, S. Chandra, and J. Mostaghimi, A Three-Dimensional Model of Droplet Impact and Solidification, *Int. J. Heat Mass Trans.*, 2002, **45**, p 2229-2242
13. J. Madejski, Solidification of Droplets on a Cold Surface, *Int. J. Heat Mass Trans.*, 1976, **19**(9), p 1009-1013
14. C. Mundo, M. Sommerfeld, and C. Tropea, Droplet-Wall Collisions: Experimental Studies of the Deformation and Breakup Process, *Int. J. Multiphase Flow*, 1995, **21**(2), p 151-173
15. C. Mundo, U. Lackermeier, M. Sommerfeld, and C. Tropea, Numerical and Experimental Studies of the Splashing and Deposition of Spray Droplets on Surfaces, *11th ILASS Europe*, Nürnberg, Germany, 1995
16. C. Escure, M. Vardelle, and P. Fauchais, Experimental and Theoretical Study of the Impact of Alumina Droplets on Cold and Hot Substrates, *Plasma Chem. Plasma Process.*, 2003, **23**(2), p 185-221
17. M. Fukumoto, E. Nishioka, and T. Nishiyama, New Criterion for Splashing in Flattening of Thermal Sprayed Particles onto Flat Substrate Surface, *Surf. Coat. Technol.*, 2002, **161**(2-3), p 103-110
18. H. Jones, Cooling, Freezing and Substrate Impact of Droplets Formed by Rotary Atomization, *J. Phys. D Appl. Phys.*, 1971, **4**(11), p 1657-1660
19. H. Guo, S. Kuroda, and H. Murakami, Microstructures and Properties of Plasma-Sprayed Segmented Thermal Barrier Coatings, *J. Am. Ceram. Soc.*, 2006, **89**(4), p 1432-1439